ChemSystemsChem

Research Article
doi.org/10.1002/syst.202200028

Chemistry Europe
European Chemical Societies Publishing

www.chemsystemschem.org

Special Collection

Engineering a Synthetic RNA Segregation System

Daniel Hürtgen,[a] Judita Mascarenhas+,[a] Mahesh A. Vibhute+,[c] Laura I. Weise,[b] Viktoria S. Mayr,[b] Victor Sourjik,*[a] and Hannes Mutschler*[c]

Cells possess a number of active segregation machineries for both chromosomal and large extrachromosomal DNA elements to avoid stochastic loss during cell division. In contrast, system that can be exploited for active, general segregation of RNA molecules including mRNAs or self-replicating RNA constructs are currently lacking. Here, we present an artificial RNA segregation system derived from the bacterial type II ParMRC plasmid segregation system and the RNA coliphage MS2. We show that fusing the partition protein ParR with the MS2 RNA coat protein enables specific binding to microbeads decorated with RNA-repeats of the archetypical MS2 RNA operator hairpin. Addition of the actin homologue ParM protein triggers efficient and rapid microbeads segregation via ATP-dependent ParM polymerization. Our new RNA partitioning system could be used for specific localization of mRNAs and/or the stable maintenance of self-replicating RNA vectors in various contexts such as living and artificial cells.

Introduction

Active DNA segregation is a key process in biology that safeguards the stable distribution of genomic information during cell division. In eukaryotic cells, dynamic spindles formed from rapidly reorganizing microtubular spindles serve as tracks for molecular motors for chromosome transport during genome segregation.[1–3] In contrast, prokaryotes evolved a more diverse range of chromosomal DNA segregation mechanisms,[4,5] in which ParA-type ATPases commonly partition chromosomal origins of replication.[6–9] Furthermore, extrachromosomal plasmids possess their own filament-based DNA segregation systems, typically containing three elements: a centromeric DNA sequence, a DNA binding protein, and an ATPase.[10–13] Most prominent classes of these partitioning systems are type I segregation systems employing ParA-type ATPases (similar to the chromosome segregating systems mentioned above), and type II segregation systems employing actin-like ATPases of the ParM-type.[10] The dynamically unstable ParM polymers consist of polar, left-handed, double-helical filaments and are tethered to the DNA at the growing end via a helical accessory protein complex.[14] The ParMRC system, which besides ParM includes the centromeric *parC* site and the *parC*-binding protein ParR, is the most thoroughly characterized prokaryotic segregation machinery[15,16] that has also been reconstituted *in vitro*.[17,18]

While diverse DNA-segregation machineries have been discovered, no dedicated partitioning mechanism for RNA molecules are known to exist. Most natural self-replicating RNA species are of transient viral origin that require no stable intracellular inheritance while vertically transmitting RNA viruses such as Narnaviruses are thought to persist due to their high copy numbers[19] or symbiotic relationships with their hosts.[20] However, dedicated segregation mechanisms might improve the efficacy of various therapeutically relevant, synthetic RNA amplicons. For example, self-replicating RNA constructs are attractive candidate for highly efficient mRNA vaccination, cancer immunotherapy, gene therapy or the generation of pluripotent stem cells.[21–24] Moreover, engineered partitioning mechanisms for non-replicative mRNAs raises the attractive possibility to control spatio-temporal activities of specific mRNAs to manipulate and study various biological processes.[25] Finally, establishing an experimental system for RNA segregation might aid the creation of artificial cells based on RNA-genomes and shed light on potential mechanisms of RNA-segregation in early protocells.[26]

Here, we set out to design and test an artificial chimeric RNA segregation system combining the bacterial ParMRC system and an RNA-binding module based on the specific interaction of the bacteriophage MS2 coat protein (MS2CP) with defined hairpin motifs. Using a chimeric fusion protein between ParR and MS2CP, we showed that hairpin repeats recognized by the phage protein induce ParM polymerisation and active segregation of RNA-coated beads.

[a] Dr. D. Hürtgen, Dr. J. Mascarenhas,+ Prof. Dr. V. Sourjik
Max Planck Institute for Terrestrial Microbiology & Center for Synthetic Microbiology (Synmikro), Karl-von-Frisch Straße 16, 35043 Marburg, Germany
E-mail: victor.sourjik@mpi-marburg.mpg.de
[b] L. I. Weise, V. S. Mayr
Max Planck Institute of Biochemistry, Am Klopferspitz 18, 82152 Martinsried, Germany
[c] Dr. M. A. Vibhute,+ Prof. Dr. H. Mutschler
TU Dortmund University, Department of Chemistry and Chemical Biology, Otto-Hahn-Str. 4a, 44227 Dortmund, Germany
E-mail: hannes.mutschler@t-dortmund.de
[+] These authors contributed equally to this work.

Supporting information for this article is available on the WWW under https://doi.org/10.1002/syst.202200028

Special Collection An invited contribution to a Special Collection on Protocells and Prebiotic Systems.

Results and Discussion

Generation of MS2CP-ParR fusion constructs

In the native ParMRC system from the R1 plasmid, ParR structurally assembles into a right-handed helix structure with the *parC* DNA-binding sites facing outward. One full turn of this helix comprises of 12 ParR dimers that facilitate binding and polymerization of ParM filaments[27] (Figure 1A). While the N-terminus of ParR is responsible for *parC* binding, its C-terminus is required for its interaction with the ParM filament.[27] To complement the DNA-binding properties of ParR with specific RNA recognition, we sought to fuse the ParR N-terminus with a specific RNA binding protein. For this, we chose the MS2 coat protein (MS2CP) from the RNA bacteriophage MS2, whose homodimer natively recognizes a specific regulatory RNA "operator" hairpin (MS2HP) structure in the bacteriophage genome.[28] To prevent MS2CP dimers from interacting cooperatively, we used an established variant carrying the mutations V75E and A81G, whose dimers can still specifically bind MS2HP but can no longer assemble into capsids and oligomers.[29] We speculated that binding of such a chimeric construct to a sufficient number of tandem MS2HP repeats would allow formation of ParR helix-structure retaining the ability to induce of ParM recruitment (Figure 1B).

To combine the RNA-binding properties of the MS2CP with the ParM-filament binding properties of ParR, we designed several fusion proteins using the available 3D structures of both proteins as starting point.[27,30] We estimated that an optimal linker length of ~27 Å between the C-terminal ParR domain and MS2CP should suffice to avoid steric clashes or folding problems of both dimeric proteins, while still enabling the anticipated ParR helix formation upon RNA binding (Supplementary Figure 1A). Test expressions of different constructs identified a soluble fusion construct with a flexible linker comprising of 15 amino acids $(GGGGS)_3$ between both proteins (MS2CP-ParR).

MS2CP-ParR specifically binds RNA containing MS2HP binding sites

To verify whether the MS2CP-ParR fusion protein binds specifically to RNAs containing the MS2HP motif, we performed an electrophoretic mobility shift assay (EMSA). We synthesized a fluorescently labelled 834 nucleotides long MS2HP RNA analogue comprising 14 MS2HP binding sites (14×MS2HP, Supplementary Figure 1A) using *in vitro* transcription reactions supplemented with 0.2% Aminoallyl-UTP-Cy5. The low average label density (~0.5/Cy5-U per RNA molecule) was expected to provide good specific visualization of the RNA construct without significantly affecting the binding properties. As a control for non-specific RNA binding, we used a fluorescently labelled sfGFP mRNA of the same length, which contains no MS2HP binding motifs for the MS2CP protein domain. To assay RNA-protein binding, we co-incubated both RNAs (100 nM) in presence of unlabelled tRNA with increasing concentrations of MS2CP-ParR (0.5–5.1 μM) before performing native gel agarose gel electrophoresis. We observed a noticeable decrease in the mobility of 14×MS2HP starting at 1.3 μM MS2CP-ParR, which continued to increase with higher protein concentrations (Figure 2A). This behaviour is well in agreement with the multiple binding sites for the MS2CP domain provided by the 14 MS2HP repeats. The specificity of the interaction was confirmed by the absence of any change in electrophoretic mobility of sfGFP mRNA even at excess concentrations of 5.1 μM MS2CP-ParR (Figure 2B).

Implementing an engineered system for RNA segregation

After verifying specific binding of MSCP-ParR to 14×MS2HP, we probed whether the fusion protein is capable of mediating RNA segregation *in vitro*. We synthesized a 3'-biotinylated variant of the 14×MS2HP *parC*-RNA analogue (14×MS2HP-bio), which was used to label streptavidin coated magnetic beads (Figure 1B). Next, we set out to probe whether the MS2CP-ParR

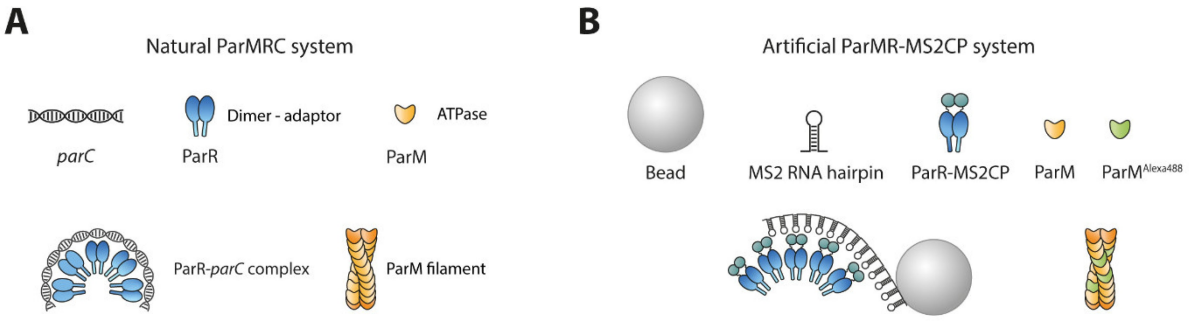

Figure 1. Design of the RNA segregation system. (A) Illustration of the natural components of the ParMRC plasmid segregation system. The ATPase ParM forms actin-like double helical filaments comprising two protofilaments, which are dynamically unstable unless capped at both ends by a DNA-bound ParR-*parC* complex. ParR dimers bind to the *parC* DNA forming a large superhelical solenoid structure (ParR-*parC* complex) that binds to the very tips of ParM filaments and prevents filament disassembly. (B) Scheme representing the design of the artificial ParMR-MS2CP RNA segregation system. ParM is supplied in two variants: the wildtype protein and an Alexa488-labeled ParM variant for visualization. ParR is fused N-terminally to the MS2 coat protein (MS2CP). Dimers of ParR-MS2CP are assumed to bind to MS2 hairpin repeats to form artificial cap structures that cause stabilization of ParM filaments similar to the natural ParR-*parC* complex.

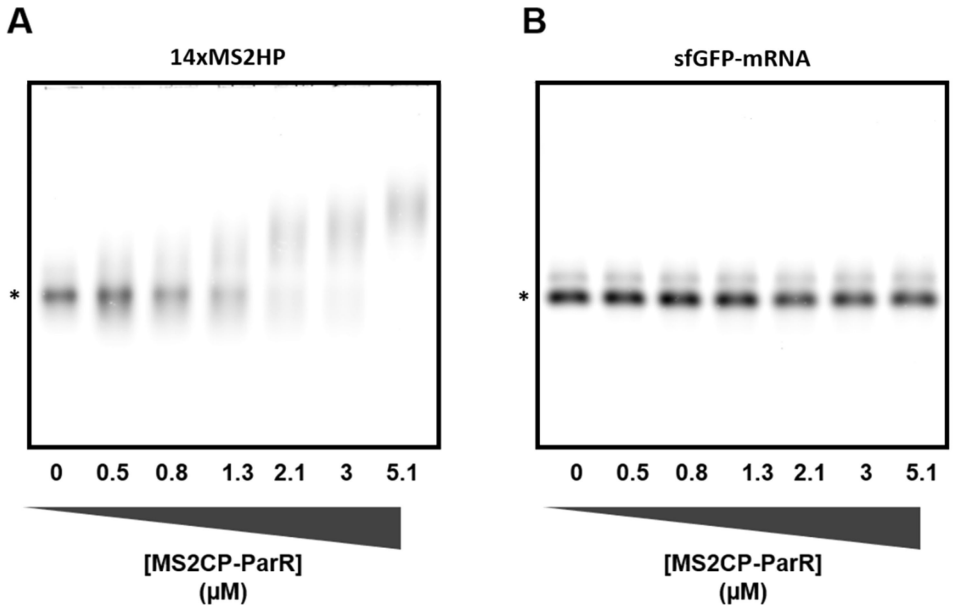

Figure 2. MS2CP-ParR binds specifically to RNA containing MS2HP motifs. Electrophoretic mobility shift assays using Cy5-labelled (A) 14×MS2HP RNA and (B) control sfGFP mRNA lacking MS2HP binding sites. Before EMSA, 100 nM RNA was equilibrated for 2 h with increasing concentrations of MS2-ParR fusion protein (0–5.1 μM) in binding buffer (see Material and Methods). Unbound RNAs (*) migrate as discrete bands. Gel electrophoresis was performed in a 1.5% TA agarose gel on ice for 3.5 hours at 1.6 V cm^{-1}.

complex with 14×MS2HP could induce ParM spindle assembly similar to the natural ParR complex with *parC* DNA, using a fluorescence-microscopy based spindle formation assay (Figure 3A).[18] To this end, 14×MS2HP-bio coated beads were mixed with an excess of MS2CP-ParR fusion protein and partially (30%) Alexa-488 labelled motor protein ParM in the presence of ATP. We observed formation of ParM asters and spindles on MS2CP-ParR bound to 14×MS2HP-bio coated beads (Figure 3B). Here, as previously,[18] the term "spindle" refers to ParM filaments that are attached in a bipolar manner to beads covered with the MS2CP-ParR complex with 14×MS2HP-bio. In contrast, the term "aster" refers to ParM filaments that are attached to such beads at one end only. Both, aster (median = 3.2 μm) and spindle length (median = 10.2 μm) of the RNA-dependent system were almost identical to the ParM filament lengths reported previously during ATP-dependent segregation of beads coated with the natural double stranded *parC* DNA motif[18] (Figure 3C). Moreover, similar as in the DNA-dependent system, an average of three asters were formed per RNA-coated bead leading to multipolar spindles interconnecting more than two beads (Figure 3C, Supplementary Figure 2). Neither ParM asters nor filaments were observed when experiments were performed either in the absence of MS2CP-ParR or with uncoated beads (Supplementary Figure 3A, B)

We further observed that beads connected via only a single spindle were actively segregated from each other in an ATP-containing reaction buffer previously used for DNA segregation[18] over a distance of 30–40 μm within ~3 minutes (Figure 4, Supplementary Figure 2, Supplementary Movie 1). This observation implied that binding of the MS2CP domain to MS2HPs allows the ParR subunit to form a protective complex that prevents catastrophic disassembly of ParM filaments. Given similar dynamics and length scales of the asters and spindles compared to the *parC* system, ParM polymerization dynamics appeared to be largely unaffected by the nature of the protein-nucleic acid interaction. Interestingly, *parC* DNA-binding capacity of ParR was preserved in the functional MS2CP-ParR fusion construct and we observed moderate aster and some spindle formation when the fusion construct and ParM were incubated in presence of ATP and *parC* DNA (Supplementary Figure 3C), although in this case ParM filamentation was less efficient when compared to the 14×MS2HP-bio coated beads (Figure 3B) or to the previously studied segregation of *parC* DNA beads by unfused ParR.[18] Consequently, while the MS2CP-ParR fusion protein has the ability to recognize both DNA and RNA elements and to initiate ParM filamentation in both cases, it has partly lost its functionality for the segregation of DNA.

Conclusion

Our work describes the successful bottom-up engineering of a chimeric cytoskeletal-based RNA segregation machinery by repurposing the R1-ParMRC plasmid segregation system through a fusion of the ParR protein with the MS2 coat protein. The fusion construct MS2CP-ParR behaved similar to the native system ParR and triggered dynamic ParM filament formation while segregating RNA-coated beads. Thus, a simple three-component system featuring ParM, MS2CP-ParR and an RNA containing a MS2HP-repeat cassette appears to be sufficient to drive polar RNA segregation *in vitro*.

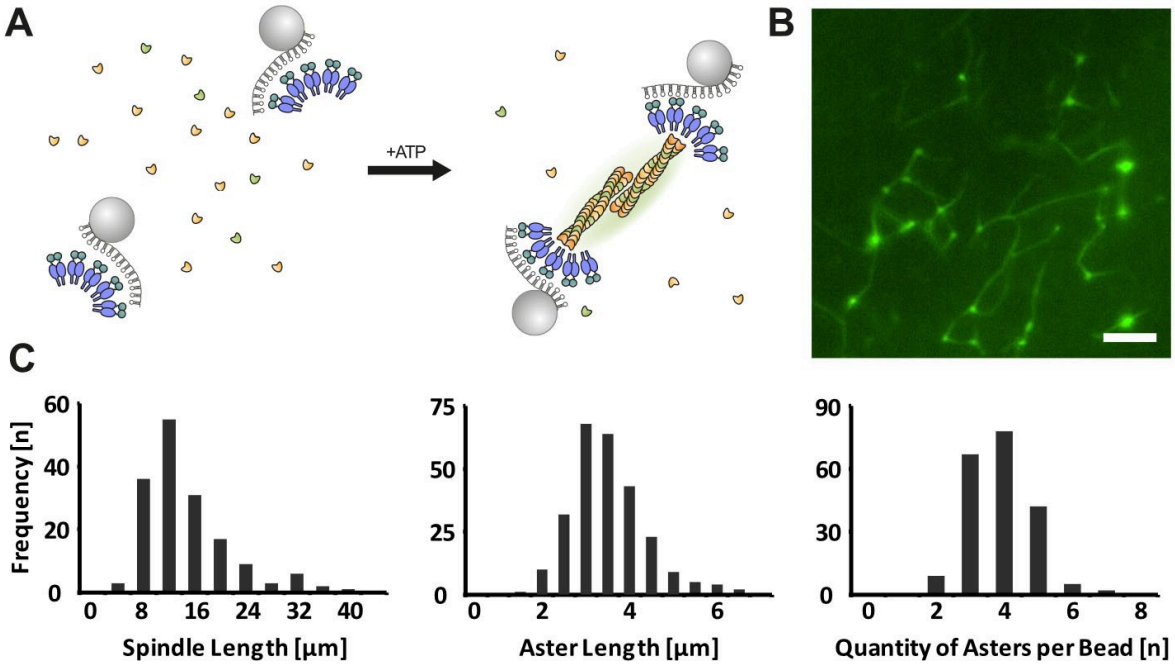

Figure 3. *In vitro* assembly of the ParR-MS2CP fusion protein filaments on RNA-coated beads. (A) Illustration of the putative mechanism for ATP-dependent ParM filament assembly leading to segregation of RNAs containing MS2HP-repeats. The filaments either become capped by a ParR-MS2CP complex with MS2 RNA hairpins followed by stable bipolar elongation or they collapse in catastrophic disassembly upon ATP hydrolysis. Incorporation of Alexa488-labeled ParM enables visualization of the filament formation. (B) Representative fluorescence microscopy image of spindle formation on RNA-coated beads. Spindle assembly was performed using 1 µM ParR-MS2CP, 5 µM ParM (30% labelled), 14 pM of 14×MS2HP-bio coated beads in presence of 10 mM ATP. Magnification: 40×; Scale bar = 10 µm. (C) Summary of statistical analysis of spindle length (left, n = 163), aster length (middle, n = 261) and quantity of asters (right, n = 203) during steady-state ParM spindle formation under conditions shown in (B).

MS2 repeats in combination with the fusion protein could be used as RNA-encoded module to improve stable inheritance of synthetic RNAs such as therapeutic RNA vectors expressing anticancer, toxic and/or immunostimulatory genes or self-amplifying RNA vaccines.[31,32] The engineered partitioning system may also be used to introduce segregation of self-replicating RNAs in cell-free environments.[26] Here, a minimized MS2-hairpin loop cassette could be used to trigger ParR/ParM-dependent segregation of RNAs in artificial compartments such as liposomes or emulsion droplets during continuous evolution experiments. Efficient segregation in these systems might help to minimize the need for strong over-amplification of typical self-replicating RNAs to ensure maintenance within compartments. In this context, segregation of RNA nanoparticles that occur as intermediates during RNA replication could be a possible strategy to enable for more distinguished foci and allow its spatial distribution via segregation.[33]

Experimental Section

Strains and plasmids

E. coli strains DH5a and BL21 (DE3) were used for cloning and protein production purposes respectively. The plasmid pET11a-parC containing *parC*, the expression plasmids pET11a-ParR and pET11a-ParM were a kind gift from Paul Buske.[17] The ParM open reading frame of this construct contains five additional amino acids (GSKCK) at the C-terminus to allow covalent attachment of fluorescent probes containing sulfhydryl-reactive functional groups. For construction of pET28a (ParR + linker + MS2CP), the coding region for R1 ParR was amplified from plasmid pKG491.[34] The coding region of MS2CP was amplified from reverse transcribed RNA of genomic wildtype MS2-RNA (Roche). Both genes were fused by a flexible linker $(GGGGS)_3$. *In vitro* transcription templates for 14xMS2-RNA were obtained from plasmid pTL032 (Addgene) and pIVEX2.3d-sfGFP, which was kindly provided by the Schwille lab (MPI Biochemistry, Martinsried, Germany)

Expression, purification and labelling of ParM

The expression of ParM, its purification and labeling was performed as described before.[18] Briefly, expression of *parM* was induced in exponentially growing *E. coli* cultures by adding lactose (final concentration 2%). After overnight expression at 30 °C, cells were harvested and lysed by sonication. The cleared lysate was treated with 10 mM ATP to induce ParM polymerization. The filaments were harvested by ultracentrifugation at 100,000x g. This step was repeated twice before the harvested ParM-pellets were disassembled in ATP-free buffer (30 mM Tris-HCl pH 7.5, 25 mM KCl, 1 mM $MgCl_2$, 2 mM DTT) and further purified by size exclusion chromatography using a Superdex S200 (GE Healthcare) gel filtration column in storage buffer (30 mM Tris-HCl pH 7, 100 mM KCl, 2 mM $MgCl_2$, 2 mM DTT). For labelling, DTT and glycerol were removed using PD10 salt exchange column equilibrated in storage buffer. For labeling, a commercially available kit was used (Alexa Fluor® 488 Protein Labeling Kit, Invitrogen). The average labeling efficiency was 90 ± 10%.

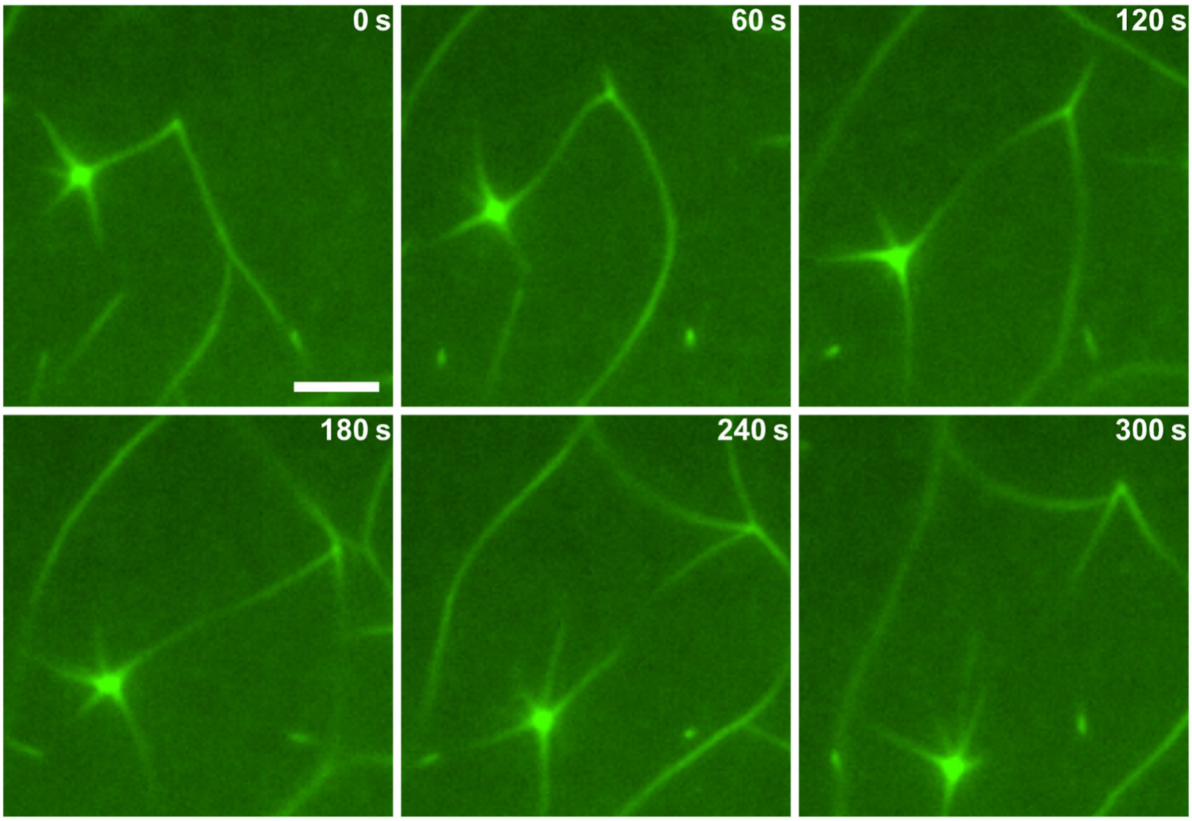

Figure 4. Dynamic segregation of RNA-coated beads mediated by the ParR-MS2CP fusion protein. Time-lapse of ParM-mediated segregation of 14×MS2HP-bio coated beads, under conditions as in Figure 2 (1 μM ParR-MS2CP, 5 μM ParM, 14 pM 14×MS2HP-bio coated beads,10 mM ATP). Scale bar = 5 μm.

Expression and purification of fusion protein

MS2CP-ParR was expressed in *E. coli* BL21(DE3) cells grown in LB medium with respective antibiotic at 37 °C, pre-conditioned with 3.3 mM sorbitol and 2.5 mM betaine to improve protein solubility. At an OD_{600} of 0.8, the cultures were shifted to 30 °C, induced with 0.1 mM IPTG and harvested after 4 h. Cell pellets were resuspended in 1x LEW-buffer (50 mM NaH_2PO_4, pH 8, 300 mM NaCl, 8 M urea) and lysed by sonication. The cleared lysate was diluted to 20 mL LEW-buffer and the fusion proteins purified using the Protino® Ni-TED 2000 Kit (Macherey-Nagel) following the manufacturer's instructions followed by a size exclusion step using a Superdex75 column (GE Healthcare Life Sciences) equilibrated in buffer R (30 mM MES pH 6.0, 300 mM KCl, 1 mM EDTA, 1 mM DTT).

Glass slide and coverslip preparation

For passivation, commercially pre-cleaned slides and coverslips were used. Slides and coverslips were further cleaned in a sonication bath with acetone, ethanol, isopropanol and DI water for 3 min each. The surface was dried under nitrogen gas jet and subsequently plasma treated using oxygen plasma (45 s). Eventually, gas phase silanization was performed o/n by placing the slides in a desiccator. Approximately 200 μL of silane (chlorotrimethylsilan, Sigma) was placed in a small beaker in the desiccator and a mild vacuum was applied. The treated glass slides were stored in a dust-free environment.

In vitro transcription and biotinylation of 14×MS2HP RNA

The coding region for 14×MS2HP RNA was PCR amplified from the plasmid pTL032 (Addgene) using the primers TAATACGACTCACTA-TAGGG and CGGGTTCATTAGATCTC. The PCR product was purified with a GeneJET DNA Purification Kit (Thermo Fisher) and used as template for *in vitro* transcription with the Transcription T7 Aid High Yield kit (Thermo Fisher) according to the manufacturer's protocol. Transcribed 14×MS2HP was purified using the RNeasy Micro Kit (Qiagen) according to the manufacturer's protocol. The resulting RNA construct contained 14 MS2 hairpins (7× GCACGAG-CAUCAGCCGUGC and 7× CGACGACGAUCACGCGUCG). 14×MS2HP was biotinylated in an overnight reaction at 16 °C by ligating pCp-biotin (Jena Bioscience) to the 3′-end of the RNA using T4 RNA Ligase 1. Briefly, a 47 μL solution of 0.5–2 μM 14×MS2HP in DMSO (10%) was incubated at 85 °C for 3 minutes. After cooling the sample on ice, RNA-biotinylation was initiated by adding 53 μL pCp ligation mix resulting in final concentrations of 1 mM pCp-biotin, 1 U/μL RNAse inhibitor (Molox), 1.35 U/μL T4 RNA Ligase 1 (NEB), 15% PEG 8000, 1 mM ATP and 1× T4 RNA Ligase reaction buffer. After overnight incubation at 16 °C, the resulting biotinylated RNA (14×MS2HP-bio) was purified using the RNeasy Micro Kit (Qiagen). RNA concentrations were determined using a Nanodrop One (Thermo Scientific) using the extinction coefficient at 260 nm calculated using OligoCalc.[35]

In vitro transcription of Aminoallyl-UTP-Cy5 labelled RNAs

DNA templates for *in vitro* transcription of 14×MS2HP and sfGFP RNA were amplified by PCR from pTL032 using the primers

TAATACGACTCACTATAGGG and CGGGTTCATTAGATCTC and from pIVEX2.3d-sfGFP using the primers GATCCCGCGAAATTAATACGACTC and TTAATGATGATGATGATGATGAGAACCCCCCCCG respectively. Both RNAs were *in vitro* transcribed from the resulting PCR products using the following composition: 30 mM Tris·HCl pH 7.8, 10 mM DTT, 2 mM spermidine, 30 mM $MgCl_2$, 5 mM NTPs (each), 2 U/ml *E. coli* inorganic pyrophosphatase (NEB), 1.6 U/µl RNase inhibitor (NEB), 1.6 U/µl T7 RNA polymerase (Thermo Fisher), 0.01 mM Aminoallyl-UTP-Cy5 (Jena Bioscience) and 100 ng DNA template. The resulting Cy5-labelled RNAs were purified using the Monarch RNA Cleanup Kit (50 µg, NEB). RNA concentrations were determined using a Nanodrop One (Thermo Scientific) using the extinction coefficient at 260 nm calculated using OligoCalc.[35]

Electrophoretic Mobility Shift Assay

Prior to Electrophoretic Mobility Shift Assay (EMSA) experiments, Cy5-labelled 14×MS2HP and sfGFP-RNA was incubated with increasing concentrations of MS2-CP in 50 mM Tris·HCl pH 8, 0.01 mg/ml tRNA, 50 µg/ml Heparin, 0.01% (v/v) IGEPAL CA630, 0.1 mM EDTA and 25 mM NaCl for 2 hours at room temperature. The binding buffer composition was adapted in a slightly modified form, from Chao *et al.*[36] Following incubation, a 6× loading buffer was added, consisting of 0.01% bromothymol blue and 80% glycerol, and the solution was loaded onto a pre-cooled 1.5% TA agarose gel (40 mM Tris, 20 mM acetic acid). Gels were then run on ice for 3.5 hours with 1.6 $V cm^{-1}$ in TA buffer before imaging using an Azure Sapphire Biomolecular Imager.

RNA-segregating spindle assembly

Centromeric RNA (14 pM 14×MS2HP-bio coated beads) was combined with 30% Alexa-488 labeled motor protein ParM (5 µM), fusion protein (1 µM), 0.4% methyl cellulose (400 cP), 5 mM DTT and 15 mg/mL BSA in buffer F. The reaction was spotted on a glass slide and the reaction started with 10 mM ATP (1/10th of the reaction volume of 100 mM ATP). To reduce oxidation, reactions were sealed with nail polish after covering with a coverslip.

Widefield fluorescence microscopy

For widefield fluorescence microscopy an inverted epifluorescence microscope was used (Nikon Eclipse Ti-U, Nikon Instrument, Japan) at 488 nm using 20× or 40× objective, respectively and with a Zyla 4.2 Plus sCMOS camera (Andor Technology Ltd, UK). The microscope was equipped with 525/50 nm and 647/57 nm mounted emission filters, respectively.

Image processing and measurement of length and quantity distributions

Microscopy images were processed using NIH Fiji ImageJ. Contrast or brightness adjustments were applied uniformly to the entire image field. The software was also used to determine spindle- and aster-length- as well as quantity of asters per bead-distributions.

Acknowledgements

The authors are grateful for the financial support by the MaxSynBio consortium, which was jointly funded by the Federal Ministry of Education and Research of Germany and the Max Planck Society. H.M. is grateful for funding by the European Research Council (ERC starting grant, RiboLife) under 802000. The authors further thank Paul J. Buske (UCSF) for providing the ParpET11a plasmids, Dr. Fan Jin (MPI Marburg) for modelling the 3D structure of the fusion protein, and Dr. A. Wagner (TU Dortmund) for help with the EMSA assay. Open Access funding enabled and organized by Projekt DEAL.

Conflict of Interest

The authors declare no conflict of interest.

Data Availability Statement

The data that support the findings of this study are available from the corresponding author upon reasonable request.

Keywords: MS2 · RNA · Protein engineering · Synthetic biology · Segregation

[1] S. Inoué, H. Sato, *J. Gen. Physiol.* **1967**, *50*, Suppl:259–92.
[2] B. Alberts, A. Johnson, J. Lewis, M. Raff, K. Roberts, P. Walter, **2002**.
[3] A. J. Hepperla, P. T. Willey, C. E. Coombes, B. M. Schuster, M. Gerami-Nejad, M. McClellan, S. Mukherjee, J. Fox, M. Winey, D. J. Odde, E. O'Toole, M. K. Gardner, *Dev. Cell* **2014**, *31*, 61–72.
[4] K. Gerdes, M. Howard, F. Szardenings, *Cell* **2010**, *141*, 927–942.
[5] D. Hürtgen, T. Härtel, S. M. Murray, V. Sourjik, P. Schwille, *Adv. Biosyst.* **2019**, *3*, 1800315.
[6] J. Møller-Jensen, J. Löwe, *Curr. Opin. Cell Biol.* **2005**, *17*, 75–81.
[7] M. Thanbichler, P. H. Viollier, L. Shapiro, *Curr. Opin. Genet. Dev.* **2005**, *15*, 153–162.
[8] K. Gerdes, J. Møller-Jensen, G. Ebersbach, T. Kruse, K. Nordström, *Cell* **2004**, *116*, 359–366.
[9] Z. Gitai, N. A. Dye, A. Reisenauer, M. Wachi, L. Shapiro, *Cell* **2005**, *120*, 329–41.
[10] K. Gerdes, J. Møller-Jensen, R. Bugge Jensen, *Mol. Microbiol.* **2000**, *37*, 455–66.
[11] G. E. Lim, A. I. Derman, J. Pogliano, *Proc. Natl. Acad. Sci. USA* **2005**, *102*, 17658–63.
[12] D. Hürtgen, S. M. Murray, J. Mascarenhas, V. Sourjik, *Adv. Biosyst.* **2019**, *3*, 1800316.
[13] D. Hürtgen, S. K. Vogel, P. Schwille, *Adv. Biosyst.* **2019**, *3*, 1800311.
[14] E. C. Garner, C. S. Campbell, R. D. Mullins, *Science* **2004**, *306*, 1021–1025.
[15] J. Salje, P. Gayathri, J. Löwe, *Nat. Rev. Microbiol.* **2010**, *8*, 683–692.
[16] A. C. Brooks, L. C. Hwang, *Plasmid* **2017**, *91*, 37–41.
[17] E. C. Garner, C. S. Campbell, D. B. Weibel, R. D. Mullins, *Science* **2007**, *315*, 1270–1274.
[18] D. Hürtgen, J. Mascarenhas, M. Heymann, S. Murray, P. Schwille, V. Sourjik, *ChemBioChem* **2019**, *20*, 633–2642.
[19] Y. Matsumoto, R. Fishel, R. B. Wickner, *Proc. Natl. Acad. Sci. USA* **1990**, *87*, 7628–7632.
[20] A. N. Espino-Vázquez, J. R. Bermúdez-Barrientos, J. F. Cabrera-Rangel, G. Córdova-López, F. Cardoso-Martínez, A. Martínez-Vázquez, D. A. Camarena-Pozos, S. J. Mondo, T. E. Pawlowska, C. Abreu-Goodger, L. P. Partida-Martínez, *ISME J.* **2020**, *14*, 1743–1754.
[21] N. Yoshioka, E. Gros, H. R. Li, S. Kumar, D. C. Deacon, C. Maron, A. R. Muotri, N. C. Chi, X. D. Fu, B. D. Yu, S. F. Dowdy, *Cell Stem Cell* **2013**, *13*, 246–254.
[22] Y. Li, B. Teague, Y. Zhang, Z. Su, E. Porter, B. Dobosh, T. Wagner, D. J. Irvine, R. Weiss, *Sci. Rep.* **2019**, *9*, 6932.
[23] Y. Li, Z. Su, W. Zhao, X. Zhang, N. Momin, C. Zhang, K. D. Wittrup, Y. Dong, D. J. Irvine, R. Weiss, *Nat. Can.* **2020**, *1*, 882–893.
[24] K. Bloom, F. van den Berg, P. Arbuthnot, *Gene Ther.* **2021**, *28*, 117–129.
[25] N. Y. Kim, S. Lee, J. Yu, N. Kim, S. S. Won, H. Park, W. Do Heo, *Nat. Cell Biol.* **2020**, *22*, 341–352.
[26] N. Ichihashi, *Ann. N. Y. Acad. Sci.* **2019**, *1447*, 144–156.

[27] J. Møller-Jensen, S. Ringgaard, C. P. Mercogliano, K. Gerdes, J. Löwe, *EMBO J.* **2007**, *26*, 4413–4422.
[28] D. S. Peabody, *EMBO J.* **1993**, *12*, 595–600.
[29] K. A. LeCuyer, L. S. Behlen, O. C. Uhlenbeck, *Biochemistry* **1995**, *34*, 10600–10606.
[30] C. Z. Ni, R. Syed, R. Kodandapani, J. Wickersham, D. S. Peabody, K. R. Ely, *Structure* **1995**, *3*, 255–263.
[31] K. Lundstrom, *Mol.* **2018**, *23*, 3310.
[32] A. B. Vogel, L. Lambert, E. Kinnear, D. Busse, S. Erbar, K. C. Reuter, L. Wicke, M. Perkovic, T. Beissert, H. Haas, S. T. Reece, U. Sahin, J. S. Tregoning, *Mol. Ther.* **2018**, *26*, 446–455.
[33] H. Kim, Y. Park, J. B. Lee, *Sci. Rep.* **2015**, *5*, 12737.
[34] K. Gerdes, S. Molin, *J. Mol. Biol.* **1986**, *190*, 269–279.
[35] W. A. Kibbe, *Nucleic Acids Res.* **2007**, *35*, W43–W46.
[36] J. A. Chao, Y. Patskovsky, S. C. Almo, R. H. Singer, *Nat. Struct. Biol.* **2008**, *15*, 103–105.

Manuscript received: August 4, 2022
Accepted manuscript online: January 22, 2023
Version of record online: February 2, 2023